Materials Advances

ROYAL SOCIETY OF CHEMISTRY

PAPER

View Article Online
View Journal | View Issue

Cite this: *Mater. Adv.*, 2024, 5, 5204

Pencil-on-paper flexible DBD plasma for surface disinfection†

Neha Kaushik, ‡[ab] Thuan Nguyen Dao, ‡[c] Minh Thu Nguyen,[c] Shweta B. Borkar,[a] Hoang Tung Nguyen,[c] Le Thi Quynh Xuan,[c] Tirtha Raj Acharya,[a] Thanh Tung Nguyen,[c] Eun Ha Choi,[a] Nagendra Kumar Kaushik *[a] and Linh Nhat Nguyen *[c]

Received 14th December 2023,
Accepted 21st April 2024

DOI: 10.1039/d3ma01122d

rsc.li/materials-advances

Herein, we demonstrate a facile, low-cost approach of using hand-drawn pencil on paper to construct a flexible dielectric barrier discharge (DBD) plasma device. The pencil trace on the paper's surface acts as the high voltage electrodes. The pencil-on-paper (PoP) plasma device could produce atmospheric pressure plasma in ambient conditions and fully operate continuously for more than 30 minutes. The flexible property of the PoP plasma allows the device to be bent without affecting the operation. The PoP plasma shows inhibition properties towards pathogenic bacteria within 120 s of treatment. This study showcases the potential of drawing pencil lead on paper as the basis for an affordable, flexible plasma device.

Introduction

While thermal technologies demonstrate efficiency in sterilizing microorganisms, they simultaneously alter food's sensory, nutritional, and functional attributes.[1,2] Several non-thermal technologies have been investigated for microbial inactivation while minimizing adverse impacts on food quality. Non-thermal methodologies involve irradiation, ultrasound, pulsed light, ultra-high-pressure, and pulsed electric fields.[3] These attempts exhibit success in microbial inactivation within food matrices. However, these methodologies have underlying limitations, including high equipment costs, remaining substances, and concerns related to consumer opinion.

Such issues can be conquered by recent applications of dielectric barrier discharge (DBD) cold plasma for disinfection of medical equipment,[4] decontamination in the food industry,[5] and healing wounds in medical therapies,[6] showcasing this technology's versatility across various fields. State-of-the-art DBD plasma devices can generate atmospheric plasma at room temperature without a gas supply or the requirement of vacuum conditions and have been widely used as a practical approach for surface treatment and disinfection.[7–13] Conventionally, DBD plasma devices consist of rigid components like metal electrodes and dielectric layers arranged in various outlines depending on different purposes.[14] Although DBD plasma has been well-developed, several drawbacks limit its use, including the limited flexibility for practical surface treatment.[15] To counteract such challenges, flexible DBD plasma has recently been developed to conform to intricate structures and irregular surfaces, enabling effective plasma treatment in complex environments. The flexibility of the plasma could provide incomparable advantages compared to rigid structure plasma sources and can be applied in various applications such as wound healing,[16] food processing,[17,18] and surface disinfection.[19] The production cost of flexible DBD plasma devices is affected by the material choice of the dielectric and conductive electrodes.

Elastic dielectric materials such as polyimide[20] and polyethylene terephthalate[21] are suitable for constructing flexible DBD plasma devices. In this regard, paper is an emerging low-cost material for flexible electronics.[22] This cellulose-based material possesses excellent dielectric properties, such as high breakdown strength, low dielectric loss, and high dielectric constant, while being capable of withstanding high temperatures up to 250 °C.[23] Various approaches, such as chemical treatment,[24] surface modification,[25] and layer stacking,[26] have been explored to enhance the dielectric properties of paper. Moreover, researchers have investigated the use of sustainable and eco-friendly paper sources, such as recycled paper and nitrocellulose-based paper, to improve paper-based electronics'

[a] *Plasma Bioscience Research Center, Department of Electrical and Biological Physics, Kwangwoon University, Seoul 01897, Republic of Korea. E-mail: kaushik.nagendra@kw.ac.kr*
[b] *Department of Biotechnology, College of Engineering, The University of Suwon, Hwaseong 18323, Republic of Korea*
[c] *Laboratory of Plasma Technology, Institute of Materials Science, Vietnam Academy of Science and Technology, 18 Hoang Quoc Viet, Cau Giay, Hanoi, Vietnam. E-mail: linhnn@ims.vast.ac.vn*

† Electronic supplementary information (ESI) available. See DOI: https://doi.org/10.1039/d3ma01122d

‡ NK and TND contributed equally to this work.

sustainability further.[27] These properties make the paper a promising alternative for dielectric materials in flexible DBD plasma[28,29]

The electrode deposition process is the main difficulty of constructing a plasma device on paper. Conventional methods for electrode deposition of thin film flexible plasma are ink-jet printing and screen-printing of conductive inks such as copper or silver on the dielectric surface.[16,30] However, the conductive inks require a post-deposition thermal sintering process at high temperatures, thus creating mild deformation on the paper structure.[31] Recently, Mazzeo *et al.* used metalized paper for DBD plasma, with the paper layer acting as the dielectric barrier and the metal layer engraved into an electrode structure.[32] The high cost of customized metalized paper and laser engraving systems could substantially increase the production cost of the DBD plasma. Therefore, despite the promising potential, the realization of a cost-effective approach for paper-based plasma devices is still unresolved.

Carbon-based materials, including graphite, graphene, and carbon nanotubes,[33] have recently received considerable attention as potential electrode materials for paper-based electronics devices[34] due to their excellent electrical conductivity,[35] thermal stability,[36] and cost-effectiveness.[37] Inspired by the advantages of paper and carbon-based conductive materials, the PoP approach is a facile solution to overcome the complexity of electrode construction and recycling the device. This method can deposit a thin layer of conductive graphite on the paper surface, which can be used as an electrode. PoP electronics is a rapidly growing research area that has garnered significant attention recently.[38–40] This emerging field uses graphite pencils to draw conductive circuits on paper, providing a low-cost, flexible, and lightweight alternative to traditional electronics. Using pencils as a drawing tool enables precise and scalable fabrication of circuits on paper, making it an ideal platform for wearable electronics and other flexible devices,[41] while offering several advantages, including its low cost, high availability, and biodegradability.[38] Advances in PoP electronics have led to the development of various applications,[42] including sensors,[43] strain gauges,[44] displays,[39] thermal electric,[45] microfluidic,[46] and energy storage devices.[47] Unlike conventional DBD plasma, which relies on a metal and rigid substrate, our PoP plasma requires only graphite and copy paper. In addition, plasma electrodes generally work at extreme conditions of high voltage with a high concentration of oxidative species, and thus the lifetime of the device is a major concern. Pencil-on-paper provides a cost-effective solution for plasma electrode construction. It can be repaired by redrawing the pencil trace or disposed of by burning. This reduces the environmental impact of electronic waste and provides a sustainable approach to electronics fabrication.

Herein, we present a novel approach using pencil-drawn graphite patterns as working electrodes and copy paper as flexible dielectric materials. The PoP structure is mounted onto a copper-grounded electrode. This study explores the feasibility of using graphite pencils to fabricate electrodes for plasma generators. Specifically, we investigate the effects of different graphite pencil grades, electrode thickness and surfaces of the papers before and after plasma generation, and the device's durability. Our results show that graphite electrodes can achieve plasma ignition performance comparable to noble metal electrodes at a much lower cost. Remarkably, we demonstrated its capability of antimicrobial sanitization, and it deactivated more than 90% of bacteria within 120 s of plasma treatment. This study provides a simple, cost-effective approach to fabricate high-performance electrodes for plasma generators and has significant potential for industrial applications.

Experimental

Construction of pencil on paper plasma

A graphite pencil with high carbon content (9B) was used to hand-draw the designed pattern on one side of a piece of printing paper (Fig. 1A). The electrode pattern was created on a computer and printed on paper. After that, we used the 9B pencil to draw over the printed pattern. The drawing pattern was repeated 25 times to enhance the conductivity of the graphite trace, which acts as the high-voltage electrode. The other side of the paper sheet was covered by polyimide tape. A sheet of copper tape was attached to the polyimide and acted as the ground electrode (Fig. 1B). The PoP plasma was powered by a customized AC power supply with a peak voltage of 2.6 kV and frequency of 6.6 kHz (Fig. 1C). The duty ratio of the AC power source was fixed at 11.6% with 40 ms on-time and 304 ms off-time (Fig. 1F).

Plasma characterizations

The current–voltage waveforms of the PoP plasma were measured using an OWON SDS8102 digital oscilloscope. Specifically, a voltage probe and a current probe (Tektronix P6015 and Tektronix 6021A, respectively) were used to measure the voltage and discharge current, respectively. A ceramic capacitor with a capacitance of 104 pF was connected in series to the ground electrode. The voltage across this capacitor was measured to calculate the number of transferred charges for plotting the Lissajous curve. The energy dissipated in a discharge cycle is defined by the area of the Q–V cyclogram. The dissipated power is then calculated as follows:[48]

$$P = EfD = f\int Q\mathrm{d}(V)D$$

where f is the frequency and D is the duty ratio.

Optical emission spectroscopy

Optical emission spectroscopy was used to detect the optical properties of the PoP plasma discharge. The OES measurement was conducted using an optical fiber connected to an Ocean Optics USB 4000 spectrometer. A small piece of quartz with dimensions of 2 × 2 cm was placed above the PoP electrode to prevent the discharge between the plasma and the optical fiber head. The optical fiber was placed perpendicular to the quartz surface to measure the emission of the discharge.

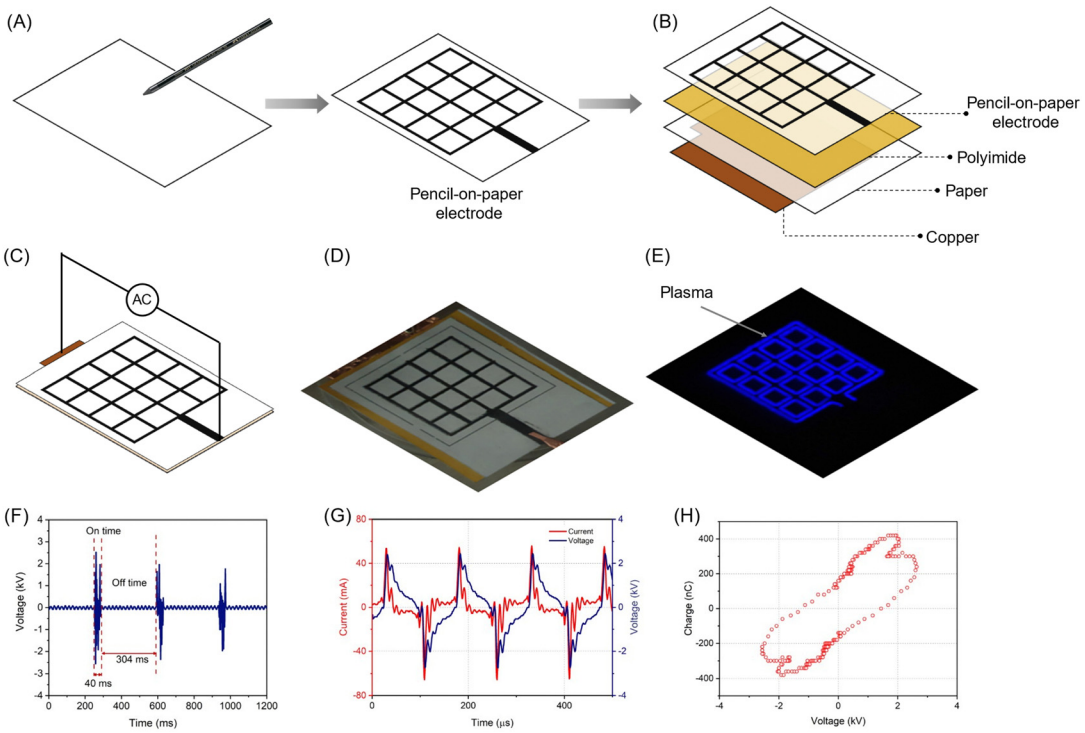

Fig. 1 Flexible plasma device made from a hand-drawn PoP plasma device. (A) The designed pattern was drawn on paper to create a PoP structure. (B) The laminated structure of the paper-based plasma device. (C) AC high voltage is applied to graphite and copper electrodes. (D) Photo of the final device. (E) Plasma generated by the device. (F) Power supply duty cycle, (G) current–voltage waveforms and (H) Lissajous curve of the device.

Ozone emission

The PoP device was placed inside a closed plastic container with dimensions of 30 × 40 × 40 cm for the ozone generation measurement using a ZE25-O3 electrochemical sensor, which was connected to a computer for data acquisition.

Scanning electron microscopic (SEM) analysis

The pencil trace morphology was measured by a JEOL-7001F scanning electron microscope (SEM), with an acceleration voltage of 15 kV. For the SEM measurement of the paper sample, a small piece of paper is mounted on the SEM holder. For the Pop device sample, firstly the device was cut into a smaller piece to fit the SEM sample holder. The measurement of all samples is carried out without any additional modification to the samples. The energy dispersive spectroscopy (EDS) elemental mapping was examined using Bruker EDS supplementary components to the SEM.

Temperature

The temperature of the PoP plasma surface before and after the operation was recorded using a Peaktech P5615 thermal imaging camera.

Antibacterial test

Bacteria culture and plasma exposure. Strains of *Escherichia coli* K-12 (*E. coli*) (KCTC-1116),[49] *Pseudomonas aeruginosa* (*P. aeruginosa*) (KCTC 1636),[50,51] and *Staphylococcus aureus* (*S. aureus*) (ATCC-12600)[52] were bought from the Korean Collection for Type Cultures (KCTC), Republic of Korea. The distance between the plasma discharge region and the agar plate was approximately 10 mm.

Exposure of pathogenic bacteria to the plasma. Bacterial cultures of *E. coli*, *S. aureus*, and *P. aeruginosa* were grown in tryptic soy broth (TSB) overnight at 37 °C, 200 rpm. The cultures were reinoculated until they reached a log phase, then diluted to 5 × 10^5 cfu mL^{-1}, and a specific volume (10 μL for *E. coli* and *S. aureus*; 5 μL for *P. aeruginosa*) of bacteria suspension was plated onto tryptic soy agar (TSA) in the whole plate. The parts of the agar plate were equally divided into control (C) and treated (T) test groups. Control experiments without plasma treatment were also conducted. Following this, the PoP plasma device was utilized to expose the half section (T) of plated bacteria with a plasma plume for 0, 30, and 120 s at 2.6 kV applied voltage along with control groups (C) from 10 mm distance. The treated bacterial plates were incubated overnight at 37 °C in an incubator. The colonies in each tested bacterial culture were counted after incubation, and the results were expressed as colony-forming units (CFUs).[53] The number of colonies of the control plate was counted because only half of the test plate was exposed to the plasma treatment and was further counted. More detailed experimental conditions are defined in Fig. 5A.

Statistical analysis

Statistical analysis was performed using PRISM 10 software with one-way ANOVA using Tukey's multiple comparison test,

where p-values less than 0.05 were considered significant. Experiments were conducted in triplicate, and results are presented as mean ± standard deviation.

Results and discussion

Plasma generation by the PoP plasma device

Generally, pencil lead consists of graphite with additives at different ratios. Based on the graphite contents, pencils are graded from 9H (lowest) to 9B (highest), with H and B standing for hard and blackness, respectively. A pencil with high graphite content can be used for drawing conductive traces on paper. In this work, we initially tested four different types of pencils (HB, 3B, 6B, 9B) to draw the conductive electrodes of the plasma device. We have measured the sheet resistivity of different pencil lead types. The obtained results show that the 9B pencil lead had the lowest sheet resistance of about 2.3 kΩ $\square^{-1}$ (Fig. S1, ESI†). Based on the measured value, we chose the 9B pencil lead for the construction of the PoP plasma electrode. Fig. 1A depicts drawing the pencil trace on the printing paper, forming the PoP structure. We sketched a 4 × 4 square pattern with 25 repetitive cycles. A thin adhesive layer coated one side of the paper, allowing the PoP structure to be attached to a dielectric substrate. The assembly process of the paper-based plasma device is shown in Fig. 1B. The device configuration was based on the dielectric barrier discharge principle between two electrodes separated by a dielectric medium while applying high-voltage AC. The PoP structure acted as the conductive electrodes. A dielectric substrate was prepared by attaching a polyimide and paper sheets. The PoP structure was adhered to the polyimide side of the dielectric substrate. Finally, a piece of copper tape was attached to the paper side of the dielectric substrate and acted as the grounded electrode. We noted that the structure of paper consists of cellulose fibers reinforced by kaolin power and is highly porous, which could allow gases to permeate the bulk volume. Therefore, there is a possibility that arc discharge could occur between the 2 electrode sides through the bulk volume of the paper layers. Thus, for the engineering of the PoP plasma device, we use the polyimide to completely separate the upper graphite electrode and the lower copper electrode. The paper-based device was powered by a high-voltage, high-frequency AC power source between two electrodes to generate the plasma (Fig. 1C). Fig. 1D demonstrates a photograph of the final paper-based plasma device. Under the applied voltage, plasma can be generated all over the pencil-drawn area (Fig. 1E and Video S1, ESI†). The current–voltage waveforms during the on-time period of the PoP device are presented in Fig. 1G. The peak voltage and discharge current were 2.6 kV and 60 mA, respectively. The average dissipate power of the PoP device was calculated from the Lissajous curve to be 1.21 W (Fig. 1H).

Variety of substrate materials, flexibility, and scalability of the PoP plasma

The PoP electrodes can be applied to various dielectric substrates, enabling flexibility and scalability of the device. To demonstrate the versatility of this approach, we adhered the PoP structure to a glass slide (Fig. 2A and B) or a single polyimide sheet to construct flexible plasma devices (Fig. 2C and D). The plasma-treated surface can be enlarged to the size of a Petri dish by changing the designed pattern of the electrodes drawn on a larger paper size (Fig. 2E–H). These results demonstrate the flexibility and scalability of our PoP DBD device. Due to the porous structure of the paper, we emphasize that the PoP structure should not be adhered directly to the copper sheet, as volume discharge between the two conductive electrodes can be generated. An additional substrate layer is required as a dielectric spacer to prevent this kind of discharge. The PoP layer can be easily peeled off and replaced with a newly drawn one. In this case, the dielectric layer and the copper sheet can be easily recycled even after the pencil lead electrode is significantly damaged. The cost of production for the PoP plasma reported in our work is much lower and easier, without the requirement of laser-engraving techniques. Moreover, our PoP plasma device can be easily repaired by redrawing the pencil trace over the damaged part.

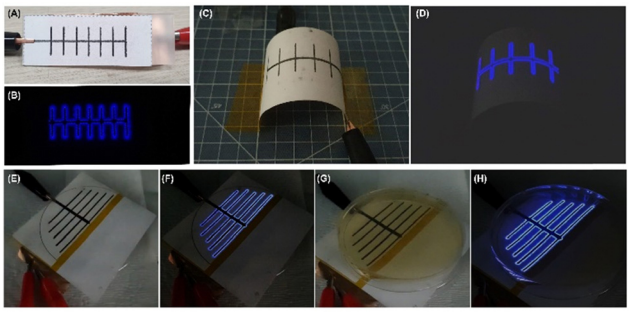

Fig. 2 The flexibility and versatility of PoP plasma: photographs of PoP electrodes on various substrate materials, showing flexibility and bending of the paper-based DBD plasma in operation: (A) and (B) glass, (C) and (D) flexible polyimide, and (E–H) large-size paper for Petri dish treatment.

Characterization of the graphite trace on paper

Scanning electron microscopy (SEM) was employed to characterize the surface morphology of the graphite trace on paper. Fig. 3A shows the surface structure of bare printed paper. We observed that the paper structure consisted of paper fibers with accumulated kaolin powders. After the drawing process, the surface of the paper is covered with smooth graphite layers (Fig. 3B). Energy-dispersive X-ray spectrometry (EDS) was employed to determine the element composition and quantify the major elements on the graphite surface. Our EDS analysis (Fig. 3G and H) indicates that four elements, C, O, Al, and Si, can be detected, with the majority element being C at almost 90%. The appearance of Al and Si can be attributed to the kaolin powder in the paper structure. The elemental mapping shows that these four elements are distributed evenly on the paper's surface, which is covered by the graphite trace (Fig. 3C–F). The thickness of each component layer was measured by cross-section SEM images (Fig. S2, ESI†). The graphite trace thickness was approximately about 55 μm. The thicknesses of the paper, polyimide, and copper layer were about 150 μm, 35 μm, and 90 μm, respectively.

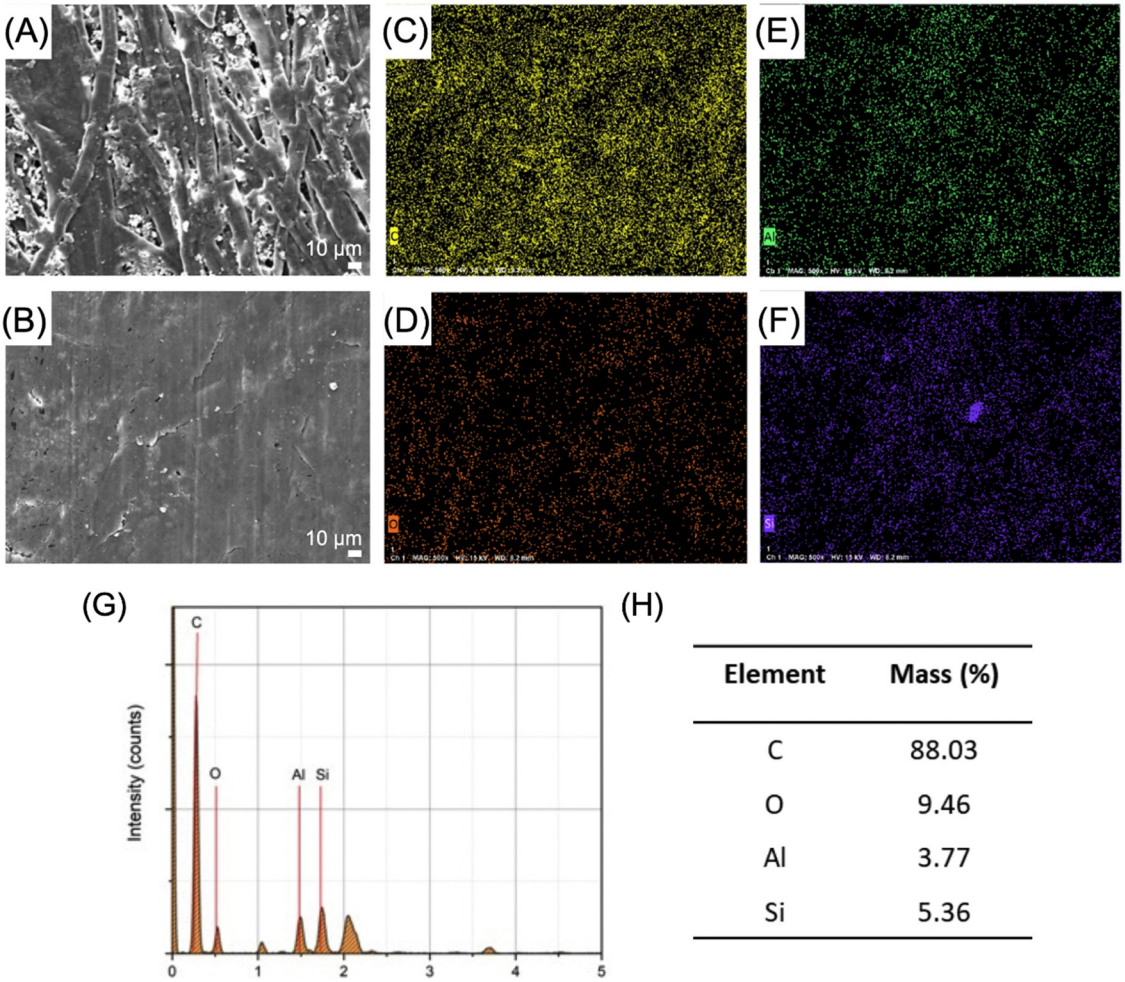

Element	Mass (%)
C	88.03
O	9.46
Al	3.77
Si	5.36

Fig. 3 Morphology and elemental composition of the PoP device surface: SEM images of the surface morphology of the paper (A) before and (B) after applying the graphite trace (by drawing). Trace analysis of the four main elements: (C) carbon, (D) oxygen, (E) aluminium, and (F) silicon on the graphite surface. (G) and (H) Analysis of element composition and quantification of the major elements on the graphite surface.

Characterization and properties of the PoP DBD plasma device

In general, one of the most crucial parameters for paper-based electronics is operational time. In this work, our paper-based plasma device can operate continuously for more than 30 minutes without disrupting plasma generation. Fig. 4A shows the temperature of the PoP plasma device surface monitored within 30 minutes of continuous operation. The surface temperature before plasma generation was recorded at 21 °C. After plasma ignition, the temperature rose from 21 to 28 °C within the first 15 minutes and stabilized between 26 °C and 28 °C during the rest of the operation. The inset photos show the detailed thermal profile images of the whole device, with the temperature at the center being 21.4 °C at the beginning, and 27.2 °C after 30 minutes of operation. We observed that while the temperature gradient was relatively homogeneous over the entire graphite electrode area, the localized temperature at the connection point between the electrode and the power supply was significantly higher (36.9 °C). We noted that due to the resistance and localized heating effect at the connection point of the graphite electrode and flat-tip crocodile clip, the temperature in this area exceeded that of the discharge region.

We measured the morphology of the pencil trace after operation to estimate electrode damage. Fig. 4B shows deformation in the surface morphology of the graphite trace after 30 minutes of plasma generation. The pencil trace surface exhibited small cracks and holes ranging in size from a few to about 20 μm, exposing the structure of the paper underneath. Previous study suggests that the chemical reaction between the electrode and oxidative substances like ozone is one of the major causes of electrode degradation. The other possible factor involves physical sputtering, where energetic particles collide with the electrode surface, leading to gradual damage. Nevertheless, these defects on the graphite surface did not affect the operation of the device, as we still observed stable plasma generation. We also emphasize that these cracks and holes can be easily repaired by drawing over new traces of pencil lead. This repairable property is a unique advantage over other commonly used methods, such as printed or deposited electrodes, where fixing broken plasma electrodes is generally

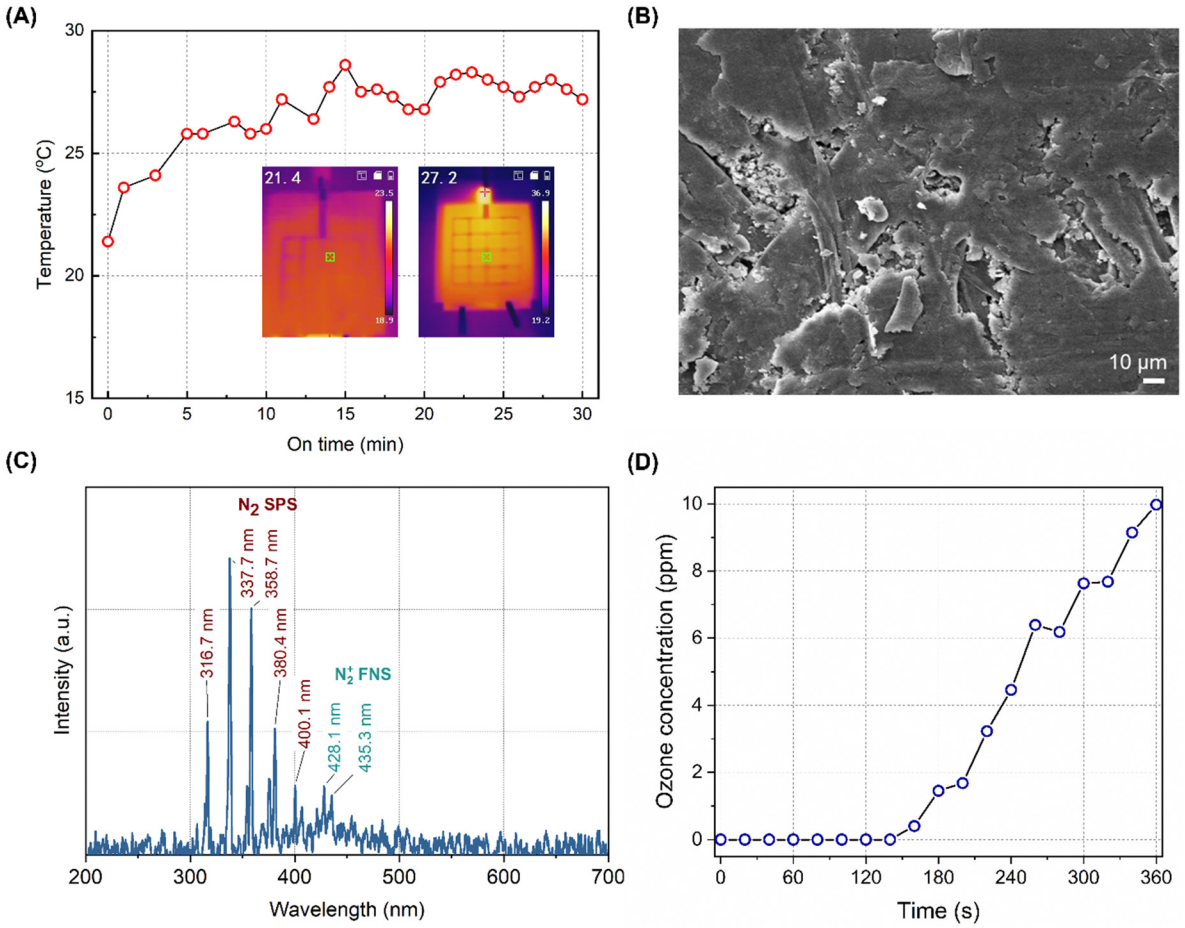

Fig. 4 Plasma operation characterizations of the PoP device: (A) temperature of the PoP plasma device temperature monitored within 30 minutes of operation (inset photo: thermal profile images of the whole device at the beginning and after 30 minutes). (B) Surface morphology of the graphite trace after plasma generation. (C) Optical emission spectrum of the generated plasma. (D) Ozone production of the paper-based plasma device over time.

considered not a viable option. Moreover, a low-duty cycle significantly contributes to the durability of the PoP device by restricting the continuous discharge time. For instance, Kim *et al.* reported that a flexible DBD plasma with silver conductive ink printed on a PET substrate could only last 6 minutes without managing the duty cycle.[21] In another work, the surface temperature of flexible plasma made from metalized paper was 60 °C after 60 s of continuous plasma activation.[32] Thus, in this work, we controlled the duty ratio (11.6%) to regulate electrode degradation and maintained the PoP surface temperature below 28 °C.

The optical emission spectrum was measured to understand the plasma reactive species generated at the discharge region (Fig. 4C). As operated in the ambient air environment, the paper-based plasma's OES showed dominant nitrogen species emissions. Specifically, intensive emission bands of the nitrogen second positive system (N_2 $C^3\Pi_u \rightarrow B^3\Pi_g$) at the band heads of 316 nm, 338 nm, 358 nm, 381 nm, and 400 nm were observed. Emissions lines of nitrogen's first negative system ($N_2^+B^2\Sigma_u^+ \rightarrow X^2\Sigma_g^+$) were also observed at 428 and 435 nm. Moreover, the PoP demonstrated excellent capability for ozone production, with a concentration of 10 ppm measured after 6 minutes of plasma treatment inside the closed environment (Fig. 4D).

Disinfection effects by the PoP plasma device

In our investigation, we assessed the bactericidal impact of PoP plasma against Gram-negative *E. coli* (K-12) and *P. aeruginosa*, as well as Gram-positive *S. aureus* (Fig. 5A). An antibacterial assay was employed to examine the growth-inhibitory response of these pathogenic bacteria to the PoP plasma, and values were determined through CFUs. Treatment with plasma exhibited a dose-dependent effect on inhibiting the growth of pathogenic bacteria. The antibacterial assay revealed a reduction in CFUs following plasma treatment. The antibacterial assay indicated that *E. coli* (K-12) growth was notably hindered at the highest exposure time of 120 s, followed by *S. aureus* and *P. aeruginosa*. The antibacterial assay (Fig. 5B and C) showed 4, 8, and 20 CFUs in *E. coli* (K-12), *S. aureus*, and *P. aeruginosa* at 120 s of exposure, respectively. For the treatment time of 30 s, we noticed a significant difference in the number of formed CFUs between the treated half (T) and the control half (T) of the Petri dish. The treated area showed a much smaller number of CFUs, indicating the efficiency of the direct treatment by PoP. In the

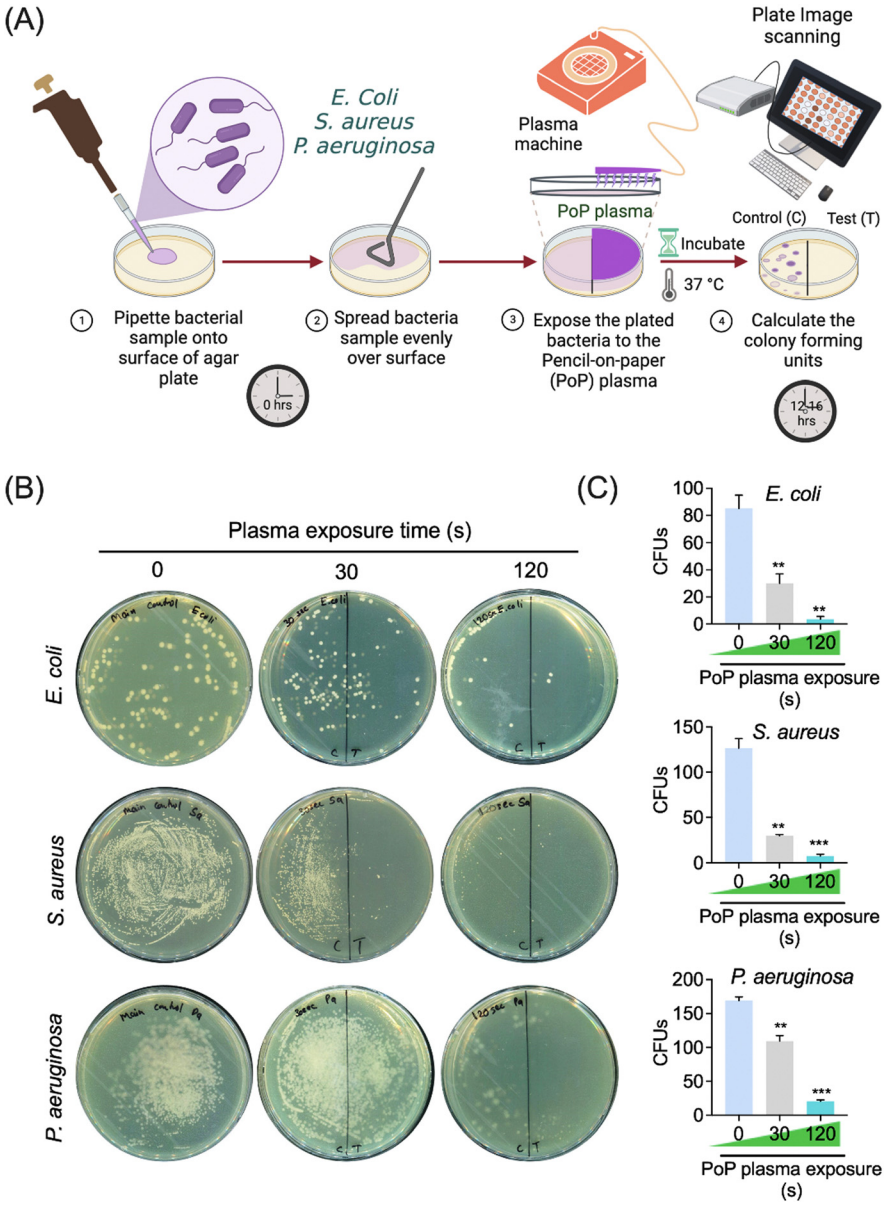

Fig. 5 PoP (PoP) exhibits antimicrobial effects. (A) Schematic presentation for the experimental setup used to perform antibacterial studies. (B) and (C) Exposure of pathogenic bacteria, for instance, *E. coli* (K-12), *S. aureus*, and *P. aeruginosa*, with PoP plasma at 30 and 120 seconds (s) and representative images of colony-forming units (CFU) of these bacteria after plasma exposure. Bar graphs show the quantitative measurement of CFU as recorded by the images observed in panel B. C represents the control group, while T represents the PoP-treated group. Tukey's multiple comparison test with one-way ANOVA was used to determine the statistical significance ** $p < 0.01$., and *** $p < 0.01$.

case of 120 s treatment, the number of CFUs in the control half was also drastically small. The decrease of CFUs in the non-exposed area could be attributed to the inactivation of bacteria by the plasma-generated ozone that accumulated in the confined space of the Petri dish. The reactive species that are generated in the plasma can deactivate the bacterial cells by oxidizing lipids in the cell membranes or by diffusing through the bacterial cell membrane and reacting with the intracellular targets. While short-life species can contribute to the bactericidal disinfection effect, long-life species should have a much more significant role. In our experiment, the plasma was generated in an air medium on the surface of the PoP device, and hence O_3 should be the most abundant long-life species, which contributes a significant role to the bactericidal effect. The obtained results demonstrate the proof-of-concept for the disinfection effect of the PoP plasma.

Conclusion

In this study, we present an innovative approach for the cost-effective fabrication of a flexible plasma device based on hand-writing pencil traces on paper. The PoP device can generate atmospheric pressure plasma in ambient air for more than

30 minutes without disruption. The PoP device can be bent due to the flexibility of the paper substrate. Notably, it can be easily repaired, recycled, or disposed of. We also examined the operation conditions of the pencil-on-paper plasma devices and presented valuable information, such as electrode degradation, electrode operation time, and ozone generation capability. The presented method is versatile for plasma device construction and can be used for various dielectric materials. The PoP plasma shows highly effective disinfection properties for *E. coli*, *S. aureus*, and *P. aeruginosa* after 120 s of treatment. We strongly believe that the pencil-on-paper for flexible plasma electrodes could be highly useful for several contingencies, for instance in emergencies, prototyping, or for education purposes.

Author contributions

NK: Investigation, visualization, writing – original draft, writing – review & editing.; TND: formal analysis, writing – original draft; TMN: investigation; SB: investigation; HTN: investigation; LTQX: investigation; TRA: investigation; TTN: resources; EHC: resources; NKK: supervision, writing – review & editing; LNN: conceptualization, funding acquisition, investigation, writing – original draft, writing – review & editing.

Conflicts of interest

There are no conflicts to declare.

Acknowledgements

This work was supported by the Vietnam Academy of Science and Technology (VAST) under the project number THTEXS.06/22-25. Linh Nhat Nguyen was funded by the Postdoctoral Scholarship Programme of Vingroup Innovation Foundation (VINIF), code VINIF.2023.STS.73. This research was funded by the National Research Foundation (NRF) of Korea, funded by the Korean government (2021R1A6A1A03038785, 2021R1F1A1055694).

Notes and references

1 G. B. Awuah, H. S. Ramaswamy and A. Economides, *Chem. Eng. Process.*, 2007, **46**, 584–602.
2 Y.-M. Huang, C.-K. Chen and C.-L. Hsu, *Food Sci. Technol. Int.*, 2020, **26**, 715–726.
3 R. Osae, G. Essilfie, R. N. Alolga, S. Akaba, X. Song, P. Owusu-Ansah and C. Zhou, *J. Sci. Food Agric.*, 2020, **100**, 2585–2599.
4 A. Sakudo, Y. Yagyu and T. Onodera, *Int. J. Mol. Sci.*, 2019, **20**, 5216.
5 Y. Ucar, Z. Ceylan, M. Durmus, O. Tomar and T. Cetinkaya, *Trends Food Sci. Technol.*, 2021, **114**, 355–371.
6 S. K. Dubey, S. Parab, A. Alexander, M. Agrawal, V. P. K. Achalla, U. N. Pal, M. M. Pandey and P. Kesharwani, *Process Biochem.*, 2022, **112**, 112–123.
7 A. S. Katsigiannis, D. L. Bayliss and J. L. Walsh, *Compr. Rev. Food Sci. Food Saf.*, 2022, **21**, 1086–1124.
8 K. G. Kostov, V. Rocha, C. Y. Koga-Ito, B. M. Matos, M. A. Algatti, R. Y. Honda, M. E. Kayama and R. P. Mota, *Surf. Coat. Technol.*, 2010, **204**, 2954–2959.
9 M. Laroussi, *Plasma Processes Polym.*, 2005, **2**, 391–400.
10 C. Ma, A. Nikiforov, N. De Geyter, R. Morent and K. Ken Ostrikov, *Curr. Opin. Chem. Eng.*, 2022, **36**, 100764.
11 Z. Xu, Y. Lan, J. Ma, J. Shen, W. Han, S. Hu, C. Ye, W. Xi, Y. Zhang, C. Yang, X. Zhao and C. Cheng, *Plasma Sci. Technol.*, 2020, **22**, 103001.
12 A. Filipić, I. Gutierrez-Aguirre, G. Primc, M. Mozetič and D. Dobnik, *Trends Biotechnol.*, 2020, **38**, 1278–1291.
13 C. Ma, A. Nikiforov, N. De Geyter, X. Dai, R. Morent and K. Ken Ostrikov, *Prog. Polym. Sci.*, 2021, **118**, 101410.
14 K. Ollegott, P. Wirth, C. Oberste-Beulmann, P. Awakowicz and M. Muhler, *Chem. Ing. Tech.*, 2020, **92**, 1542–1558.
15 V. I. Gibalov and G. J. Pietsch, *J. Phys. D: Appl. Phys.*, 2000, **33**, 2618.
16 N. Kim, S. Lee, S. Lee, J. Kang, Y.-A. Choi, J. Park, C.-K. Park, D. Khang and S.-H. Kim, *Adv. Sci.*, 2022, **9**, 2202800.
17 D. D. Jayasena, H. J. Kim, H. I. Yong, S. Park, K. Kim, W. Choe and C. Jo, *Food Microbiol.*, 2015, **46**, 51–57.
18 Q. Wang, R. K. Pal, H.-W. Yen, S. P. Naik, M. K. Orzeszko, A. Mazzeo and D. Salvi, *Food Control*, 2022, **137**, 108915.
19 G. S. Dijksteel, M. M. W. Ulrich, M. Vlig, A. Sobota, E. Middelkoop and B. K. H. L. Boekema, *Ann. Clin. Microbiol. Antimicrob.*, 2020, **19**, 37.
20 Y. Sun, B. Zhang, C. Wang and G. Zhang, *Adv. Electron. Mater.*, 2021, **7**, 2100369.
21 J. Kim, S. Park and W. Choe, *Sci. Rep.*, 2021, **11**, 12206.
22 Y. Zhang, L. Zhang, K. Cui, S. Ge, X. Cheng, M. Yan, J. Yu and H. Liu, *Adv. Mater.*, 2018, **30**, 1801588.
23 S. Soares, G. Camino and S. Levchik, *Polym. Degrad. Stab.*, 1995, **49**, 275–283.
24 A. M. A. Nada, M. El-Sakhawy, S. Kamel, M. A. M. Eid and A. M. Adel, *Carbohydr. Polym.*, 2006, **63**, 113–121.
25 S. Vaswani, J. Koskinen and D. W. Hess, *Surf. Coat. Technol.*, 2005, **195**, 121–129.
26 V. T. Morgan, *IEEE Trans. Dielectr. Electr. Insul.*, 1998, **5**, 125–131.
27 A. Sudheshwar, N. Malinverno, R. Hischier, B. Nowack and C. Som, *Resour., Conserv. Recycl.*, 2023, **189**, 106757.
28 C.-C. Hsu, J.-H. Tsai, Y.-J. Yang, Y.-C. Liao and Y.-W. Lu, *J. Microelectromech. Syst.*, 2012, **21**, 1013–1015.
29 Y.-J. Yang and C.-C. Hsu, *J. Microelectromech. Syst.*, 2013, **22**, 256–258.
30 J. S. Lim, D. Kim, S. Ki, S. Mumtaz, A. M. Shaik, I. Han, Y. J. Hong, G. Park and E. H. Choi, *Int. J. Mol. Sci.*, 2023, **24**, 4638.
31 S. Sato, K. Nishida, T. Hirai, M. Ito, H. Teramae, M. Matsubara, K. Kanie and N. Ohnishi, *Sens. Actuators, A*, 2022, **344**, 113751.
32 J. Xie, Q. Chen, P. Suresh, S. Roy, J. F. White and A. D. Mazzeo, *Proc. Natl. Acad. Sci. U. S. A.*, 2017, **114**, 5119–5124.

33 W. Yang and C. Wang, *J. Mater. Chem. C*, 2016, **4**, 7193–7207.
34 Y. Z. N. Htwe and M. Mariatti, *J. Sci.: Adv. Mater. Devices*, 2022, **7**, 100435.
35 R. Sanjinés, M. D. Abad, C. Vâju, R. Smajda, M. Mionić and A. Magrez, *Surf. Coat. Technol.*, 2011, **206**, 727–733.
36 X. Guo, S. Cheng, W. Cai, Y. Zhang and X. Zhang, *Mater. Des.*, 2021, **209**, 109936.
37 A. O. Egbedina, O. P. Bolade, U. Ewuzie and E. C. Lima, *J. Environ. Chem. Eng.*, 2022, **10**, 107260.
38 Y. Xu, G. Zhao, L. Zhu, Q. Fei, Z. Zhang, Z. Chen, F. An, Y. Chen, Y. Ling, P. Guo, S. Ding, G. Huang, P.-Y. Chen, Q. Cao and Z. Yan, *Proc. Natl. Acad. Sci. U. S. A.*, 2020, **117**, 18292–18301.
39 N. Kurra and G. U. Kulkarni, *Lab Chip*, 2013, **13**, 2866–2873.
40 H. Moriwaki and T. Kamine, *ACS Appl. Mater. Interfaces*, 2023, **15**, 4781–4788.
41 Y. Xu, Q. Fei, M. Page, G. Zhao, Y. Ling, S. B. Stoll and Z. Yan, *iScience*, 2021, **24**, 102736.
42 Y. Xue, Z. Wang, A. Dutta, X. Chen, P. Gao, R. Li, J. Yan, G. Niu, Y. Wang, S. Du, H. Cheng and L. Yang, *Chem. Eng. J.*, 2023, **465**, 142774.
43 G. Niu, Z. Wang, Y. Xue, J. Yan, A. Dutta, X. Chen, Y. Wang, C. Liu, S. Du, L. Guo, P. Zhou, H. Cheng and L. Yang, *Nano Lett.*, 2023, **23**, 1252–1260.
44 C.-W. Lin, Z. Zhao, J. Kim and J. Huang, *Sci. Rep.*, 2014, **4**, 3812.
45 R. Mulla, D. R. Jones and C. W. Dunnill, *Adv. Mater. Technol.*, 2020, **5**, 2000227.
46 Y. Lu, W. Shi, L. Jiang, J. Qin and B. Lin, *Electrophoresis*, 2009, **30**, 1497–1500.
47 F. Brunetti, A. Operamolla, S. Castro-Hermosa, G. Lucarelli, V. Manca, G. M. Farinola and T. M. Brown, *Adv. Funct. Mater.*, 2019, **29**, 1806798.
48 J. Kriegseis, B. Möller, S. Grundmann and C. Tropea, *J. Electrost.*, 2011, **69**, 302–312.
49 S. Makvana and L. R. Krilov, *Pediatrics In Review*, 2015, **36**, 167–171.
50 G. P. Bodey, R. Bolivar, V. Fainstein and L. Jadeja, *Rev. Infect. Dis.*, 1983, **5**, 279–313.
51 S. Qin, W. Xiao, C. Zhou, Q. Pu, X. Deng, L. Lan, H. Liang, X. Song and M. Wu, *Signal Transduction Targeted Ther.*, 2022, **7**, 199.
52 Y. C. Tong Steven, S. Davis Joshua, E. Eichenberger, L. Holland Thomas and G. Fowler Vance, *Clin. Microbiol. Rev.*, 2015, **28**, 603–661.
53 M. Ortoneda, S. O'Keeffe, J. D. Cullen, A. I. Al-Shamma'a and D. A. Phipps, *J. Microwave Power*, 2007, **42**, 13–23.